Contactless DC Connector Based on GaN LLC Converter for Next-Generation Data Centers

Yusuke Hayashi, Hajime Toyoda, Toshifumi Ise, *Member, IEEE*, and Akira Matsumoto

***Abstract*—An inductively coupled contactless dc connector has been proposed for the next-generation 380-V dc distribution system in data centers. A LLC resonant dc–dc converter topology with gallium nitride (GaN) power transistors has been applied to realize the short-distance highly efficient contactless power transfer. A prototype of a 1.2-kW 384- to 192-V connector has been fabricated and the conversion efficiency of over 95% with the power density of 8.1 W/cm^3 has been confirmed experimentally under 1000-kHz operation. The design consideration has been carried out and the potential to achieve 10.0 W/cm^3 has been also shown taking the feature of the GaN power device and the characteristics of the magnetic core material for the transformer into account. The contactless dc connector integrates the functioning of an isolated dc–dc converter into a connector for space saving, and the dc current can be cut off without arc because of the inductive coupling. The proposed connector contributes to realizing a highly efficient, space saving, and reliable future 380-V dc distribution system.**

***Index Terms*—Contactless power supply, dc power distribution, dc–dc power converters, gallium nitride (GaN).**

I. Introduction

THE amount of network traffic in the data centers and the telecommunications buildings has recently been rapidly increasing due to the widespread use of information and communication technology (ICT) equipment [1]. Energy and resource conservation in these buildings and data centers will contribute to solving some of our global environmental problems. Since 2008, the Nippon Telegraph and Telephone Group has been developing 380-V DC distribution system that goes beyond the conventional 48-V dc distribution system to realize highly efficient and space-saving (high power density) power supply system [2]–[5].

Highly efficient and ultracompact power converters are attractive to realize the high power density dc distribution system. The power density of power converters has been increasing over the past few decades and the power converters with more than 10 W/cm^3 have been already reported for dc power systems [6]–[8]. The high power density converter contributes to not only achieving its performance improvement in the conventional system but also the development of the totally optimized novel dc distribution system.

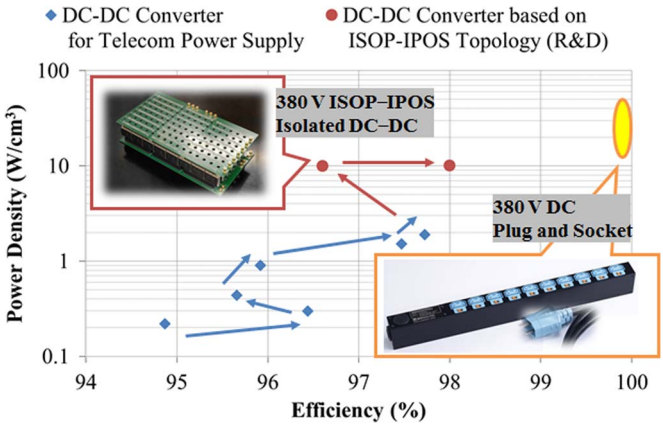

Fig. 1. Power density roadmap for isolated dc–dc converters for telecom power supply and dc connector for 380-V dc distribution system.

The dc distribution system for accomplishing higher power density has been proposed taking the input series and output parallel (ISOP) and input parallel and output series (IPOS) combination of high power density dc–dc converters into account [9]. There are two key features, as follows.

- A high-voltage (HV) ac–dc converter that consists of low-voltage ac–dc converters with series-parallel connection topology is installed to remove a distribution transformer.
- Inductively coupled contactless dc connectors (ICCCs) are utilized to reduce the total volume caused by the isolated dc–dc converter as power supply units (PSUs) and the conventional metal contact connector. Functions of the galvanic isolation and the voltage transformation are inherited to the ICCC.

The high power density ac–dc converter without the distribution transformer is a part of the solid state transformer and their performances have been already reported [10], [11]. The contactless power supply technology for dc connectors has been also reported [12], [13]. However, the application effect of the contactless connector has not been discussed in terms of the power density for the future dc distribution system.

In this paper, the feasibility of high power density ICCC is investigated quantitatively. The dc distribution system using the ICCCs is introduced in Section II. Then, details of the circuit configuration and characteristics of the connector are described in Section III. In Section IV, the design consideration for the

Manuscript received July 13, 2014; revised October 21, 2014; accepted December 17, 2014. Date of publication January 5, 2015; date of current version July 15, 2015. Paper 2014-IPCC-0529.R1, presented at the International Power Electronics Conference (IPEC-Hiroshima 2014 ECCE-ASIA), Hiroshima, Japan, May 18–21, and approved for publication in the IEEE TRANSACTIONS ON INDUSTRY APPLICATIONS by the Industrial Power Converter Committee of the IEEE Industry Applications Society.

Y. Hayashi, H. Toyoda, and T. Ise are with Osaka University, Osaka 565-0871, Japan (e-mail: y_hayashi@eei.eng.osaka-u.ac.jp; toyoda@pe.eei.eng.osaka-u.ac.jp; ise@eei.eng.osaka-u.ac.jp).

A. Matsumoto is with NTT Facilities, Tokyo 170-0004, Japan (e-mail: matsumo86@ntt-f.co.jp).

Color versions of one or more of the figures in this paper are available online at http://ieeexplore.ieee.org.

Digital Object Identifier 10.1109/TIA.2014.2387481

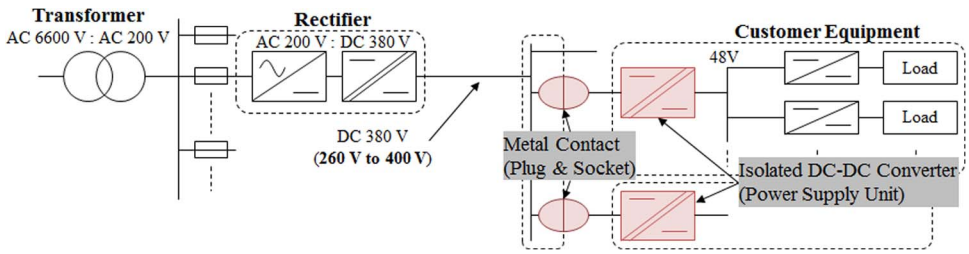

Fig. 2. Configuration of conventional 380-V dc distribution system.

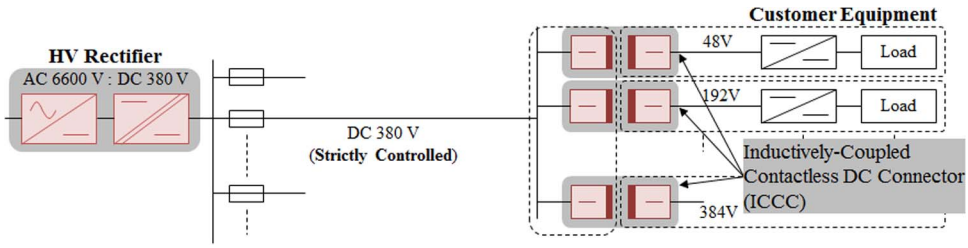

Fig. 3. Configuration of next-generation 380-V dc distribution system using contactless dc connector.

connector is conducted to show the potential for achieving high power density taking the characteristics of the gallium nitride (GaN) power device and the magnetic core material of the transformer into account. In Section V, a prototype of the contactless dc connector is fabricated based on the design consequence and the validity of the design is experimentally verified under 1.2-kW 384- to 192-V 1-MHz operation.

II. Next-Generation 380-V DC Distribution System Using ICCC

A. ICCC Concept to Realize Higher Power Density 380 V-DC Distribution System

Fig. 1 shows the power density trend of isolated dc–dc converters for the telecom power supply. In research and development stage, power converters with 10 $\mathrm{W/cm^3}$ has been already developed for 380-V dc distribution system [14]. The power density of a connector for the 380-V dc distribution system is also shown in Fig. 1. The volume of a socket for a connector is 100 $\mathrm{cm^3}$, and the power density per single socket is 10 $\mathrm{W/cm^3}$ in the case of the output power of 1 kW.

Fig. 2 shows the schematic diagram of the conventional 380-V dc distribution system for data centers. In Fig. 2, connectors with metal contacts and isolated dc–dc converters such as PSU are installed in the 380-V dc distribution line behind the rectifier. The power density of the converters is now at a level of 10 $\mathrm{W/cm^3}$, and the highly integrated converters over 50 $\mathrm{W/cm^3}$ are now commercially available for the lower voltage application as the on-board power supply [15]. The influence of peripherals will become obvious in near future.

Fig. 3 shows the schematic diagram of the proposed next-generation 380-V dc distribution system with ICCCs. The strictly controlled dc 380 V is delivered by a HV rectifier that consists of conventional rectifiers connected in ISOP-IPOS without the distribution transformer. Several levels of dc voltages are provided to loads through the ICCCs, which a conventional metal contact connector and an isolated dc–dc converter are integrated into single hardware. In Fig. 3, the dc voltages of 48, 192, and 384 V are considered for ICT servers, storage systems and lightings, respectively. These voltages are converted from the input voltage of 384 V by changing the turn ratio of the primary and the secondary windings of the transformer or the ISOP-IPOS connection topology with low-voltage converters. Here, primary and a secondary circuits of an isolated dc–dc converter are utilized as a pair of a socket and a plug for the connector, respectively. The electric power is delivered from the primary circuit to the secondary circuit through the inductive coupling in the short distance.

TABLE I
Power Densities of Installed Components in 380-V DC Distribution System

	Current 380 V DC Distribution		Next Generation DC Distribution	
	Component	$\mathrm{W/cm^3}$	Component	$\mathrm{W/cm^3}$
AC Interface	Transformer	0.66	HV–Rectifier	0.95
	Rectifier	0.95		
DC Interface	Connector	10.0	Contactless–DC Connector	10.0
	PSU	10.0		

Table I shows the power densities of installed components in the already developed 380-V dc distribution system and the proposed dc distribution system using the ICCC. By employing the contactless dc connector, the power density in the dc interface can be improved ideally from 5.0 $\mathrm{W/cm^3}(=(10.0\times10.0)/(10.0+10.0))$ to 10.0 $\mathrm{W/cm^3}$ in case the isolated dc–dc converter with the power density of 10.0 $\mathrm{W/cm^3}$ is directly utilized for the connector because the volume of the conventional connector does not have to be considered. This means that the high power-density-isolated dc–dc converter has the potential to improve not only its power density but also the power density of the whole dc distribution system.

B. Operating Condition and Required Performance of ICCC

Environment of the 380-V dc distribution system affects the specifications of the ICCC significantly. The characteristics of

the next-generation 380-V dc distribution system related to the ICCC are as follows.

- Installed loading apparatus is known. The ICT equipment as the servers and the backup power system are mainly assumed and its electrical behavior is also well-known.
- The connection and the disconnection of the ICT equipment are infrequent. These actions are mainly conducted in the case of the trouble and the scheduled maintenance.
- The installed loads are utilized in a room. The ambient temperature and the humidity are strictly controlled by the external air-conditioning machines.

Usage environment of the ICCC are summarized as follows taking the aforementioned characteristics into account.

- Electric power through the connector is basically stable and the load variation is infrequent.
- The operating temperature and the humidity are stable. The forced-convection cooling is available for the connector because of the air-conditioning equipment in the room.
- The input voltage of nominal dc 380 V for the ICCC can be strictly controlled by the HV Rectifier (the HV ac–dc converter) in Fig. 3.
- The output voltage of the ICCC has some options. Servers require dc 48 V mainly and lightings for dc 380 V are now developed. The dc 192 V can be utilized for the battery packs of the UPSs and storages.
- The primary and the secondary circuits of the ICCC are fixed as a pair of a socket and a plug of a conventional metal contact connector. This means that the primary and the secondary magnetic cores of the transformer can be aligned, and its air gap can be also kept constant to keep the coupling coefficient high.

For aforementioned environment, the LLC resonant dc–dc converter topology has been applied for the ICCC. The highly efficient and high power density connector will be developed by taking the following features into account.

- High efficiency can be achieved by zero-voltage switching (ZVS) of the main switches and zero-current switching (ZCS) of the rectifier diodes. The commercially available isolated dc–dc converter based on the LLC topology has achieved the maximum efficiency of 98% and the power density of several tens of $\mathrm{W/cm^3}$[15].
- ISOP and IPOS topologies are available in the LLC converter topology [16]. Low-voltage converters are available to develop an arbitrarily HV connector under high-frequency operation. The passive component's volume can be minimized by high-frequency operation, and the possibility of the ICCC design is expanded.
- The constant switching frequency operation is available. The voltage regulation by using pulse-frequency modulation (PFM) control is not necessary to compensate the input voltage fluctuation because the input voltage of the connector is regulated by HV rectifier in Fig. 3. The constant frequency contributes to achieving high power density because the circuit parameters can be minimized.
- The ICCC is also available for the current limiter in the overload condition. This function has the potential to realize higher power density dc distribution system taking volumes of the protection devices as dc fuses into account.

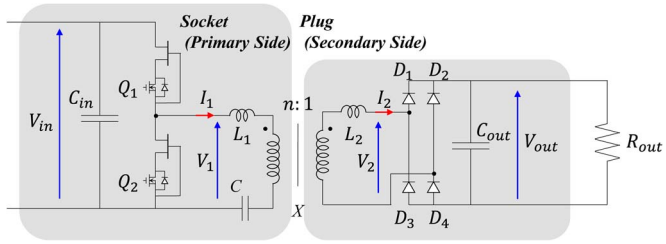

Fig. 4. Circuit configuration of contactless dc connector based on LLC resonant converter topology.

III. Contactless DC Connector Based on LLC Resonant Converter Topology

Here, circuit parameter design of a 384- to 192-V 1.2-kW ICCC is conducted under 1-MHz switching operation. Possible semiconductor power devices and the magnetic core material of the transformer are also introduced for the prototyping.

The ICCC with the aforementioned input and output voltages is available for the dc 192-V UPS and storages. Moreover, the 384 V-192-V ICCC simplifies the LLC half-bridge converter design because of the transformer turn ratio of 1.0. Based on the ISOP-IPOS topology, this connector is also available for the 384-V lighting application by connecting two converters in IPOS [9]. Ultimately, ICCCs whose output voltages are dc 48 V, dc 192 V, and dc 384 V, as shown in Fig. 3 can be developed by using 48 V-48 V isolated dc–dc converters connected in ISOP-IPOS [16].

A. Circuit Configuration and Parameter Design

The circuit configuration of the LLC converter for the connector is shown in Fig. 4. The availability of the LLC converter has been reported and this topology has been already applied for the wireless power transfer [17], [18]. The ZVS of transistors and the ZCS of diodes achieve high efficiency. In the case where the turn ratio of the transformer n is 1, the voltage gain M and the phase angle θ are calculated by following (1) and (2)

$$M = \left|\frac{V_2}{V_1}\right| = \left|\frac{s^2 N_1}{s^3 D_1 + s^2 D_2 + s D_3 + D_4}\right| \tag{1}$$

$$D_1 = \{L_1 L_2 + (L_1 + L_2) L_m\} C, \quad D_2 = R(L_1 + L_m) C$$
$$D_3 = (L_2 + L_m), \quad D_4 = R, \quad N_1 = R L_m C$$

$$\tan\theta = \frac{N_2' D_1' - N_1' D_2'}{N_1' D_1' + N_2' D_2'} \tag{2}$$

$$D_1' = -\omega^2 (L_2 + L_m) C, \quad D_2' - \omega R C$$
$$N_1' = R - \omega^2 R (L_1 + L_m) C$$
$$N_2' = -\omega^3 \{L_1 L_2 + (L_1 + L_2) L_m\} C$$

$$L_1 = \frac{1-k}{k} L_m + L_{ex}, \quad L_2 = \frac{1-k}{k} L_m, \quad R = \frac{\pi^2}{8} R_{\mathrm{out}}. \tag{3}$$

Parameters V_1 and V_2 in (1) are the input and output voltages of the LLC resonant tank in Fig. 4, respectively. The inductance at the primary side of the transformer is L_1 and this inductance L_1 includes the leakage inductance of the transformer and the

TABLE II
CIRCUIT PARAMETERS FOR CONTACTLESS DC CONNECTOR BASED ON LLC RESONANT CONVERTER TOPOLOGY

Symbol	Meaning	Value
P_{out}	Output power	1,200 W
V_{in}, V_{out}	Input / output voltage	384 V / 192 V
f_{rL}, f_{rH}	Resonant frequency	450 kHz, 1,100 kHz
f_{sw}	Switching frequency	1,000 kHz
k	Coupling coefficient	0.98
L_m	Magnetizing inductance	9.8 μH
L_1, L_2	Resonant inductance	1.6 μH, 0.2 μH
C	Resonant capacitance	11.7 nF
n	Turn ratio	1

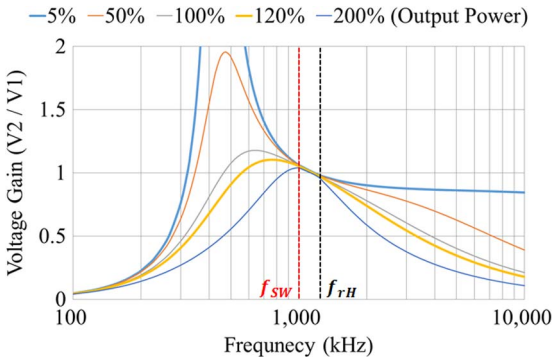

Fig. 5. Voltage gain characteristics of LLC resonant circuit in contactless dc connector.

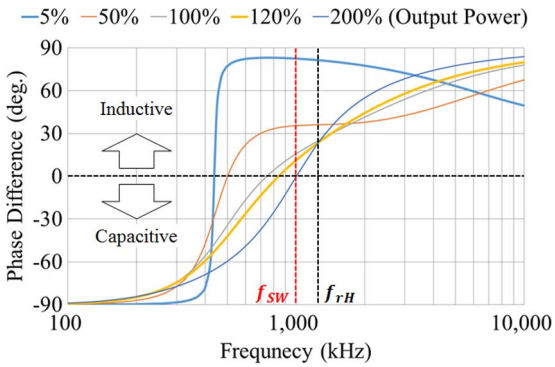

Fig. 6. Phase angle characteristics of LLC resonant tank (positive value: inductive, negative value: capacitive).

external resonant inductance L_{ex}. The inductance L_2 means the leakage inductance of the transformer. The magnetizing inductance of the transformer is L_m and the coupling coefficient is k. The resonant capacitance is C and R means the equivalent load resistance in the fundamental harmonic approximation (FHA) [19]. In case that the coupling coefficient of the transformer k is high by using the magnetic core transformer, the influence of L_2 on the voltage gain M is negligible.

Parameters to realize the contactless dc connector based on the LLC resonant converter topology are shown in Table II. Figs. 5 and 6 show the calculation results of the voltage gain M and the phase angle θ of the circuit impedance in the LLC resonant tank, respectively. The voltage gain M was drawn when the switching frequency $f_{\rm SW}$ varied from 100 kHz to 10 MHz. The phase angle θ was also drawn for the switching frequency. In Fig. 6, the positive value means the impedance has the inductive characteristics because the phase angle of the current has the delay against that of the voltage. The voltage gain and the phase angle were drawn when the output power changed from 5% to 200%. Here, the output power of 100% means the rated power of 1200 W in Table II.

In the ICCC application in the next-generation 380-V dc distribution system, its output voltage does not have to be compensated under the input voltage disturbances because the input voltage of the connector can be controlled strictly by the HV rectifier in Fig. 3. This means that the PFM for the voltage regulation is not necessary, and the switching frequency can be fixed. This contributes to achieving higher power density because of the minimization of circuit *LC* parameters without taking the frequency swing into account.

The soft switching operation has to be achieved in the LLC circuit to accomplish the high efficiency. For the ZVS soft switching operation during the turn on of the main switch Q, the impedance of the LLC resonant circuit has to be the inductive characteristics (i.e., the phase angle θ must have the positive value in Fig. 6). For the ZCS soft switching operation of the rectifier diode D, the switching frequency $f_{\rm SW}$ has to be less than the resonant frequency $f_{\rm rH}$. Here, the resonant frequency $f_{\rm rH}$ was set at 1100 kHz for the switching frequency $f_{\rm SW}$ of 1000 kHz. By setting the frequency $f_{\rm SW}$ close to $f_{\rm rH}$, the voltage gain M were kept at an approximately constant value for the load variations from 5% to 200%.

Circuit parameters of L_1, L_2, L_m and C are designed to keep the LLC impedance characteristics inductive for the variable output power. Parameters in Table II were determined to achieve ZVS and ZCS for 5% to 200% output power at the frequency of 1.0 MHz, as shown in Fig. 6.

The magnetizing inductance L_m was determined to suppress the magnetizing current $I_{\rm Lm}$, as shown in (4). Here, the peak magnetizing current was set at 4.9 A under the peak resonant current was 9.8 A calculated by the FHA analysis at 1.2-kW output power. The inductance L_1 consists of the leakage inductance and the external inductance $L_{\rm ex}$. Equation (5) shows the calculation result for L_1 with the external inductance of 1.4 μH and the coupling coefficient of 0.98. The inductance L_2 means the leakage inductance and this is calculated as 0.2 μH.

The resonant capacitance C was designed in order that the resonant frequency $f_{\rm rH}$ corresponded to the designated frequency of 1100 kHz, as shown in (6). The capacitance C was calculated as 11.7 nF by using aforementioned L_1, L_2, L_m, and $f_{\rm rH}$

$$L_m = \frac{V_1 \Delta t}{\Delta I_{Lm}} = \frac{384V}{2} \cdot \frac{1}{2 \cdot 1MHz} \cdot \frac{1}{2 \cdot 4.9A} \cong 9.8\mu\text{H} \quad (4)$$

$$L_1 = \frac{1-k}{k} L_m + L_{ex} = \frac{0.02}{0.98} 9.8\mu\text{H} + 1.4\mu\text{H} \cong 1.6\mu\text{H} \quad (5)$$

$$f_{\rm rH} = \frac{1}{2\pi} \sqrt{\frac{L_2 + L_m}{\{L_1 L_2 + (L_1 + L_2) L_m\} C}}. \quad (6)$$

Here, the peak magnetizing current and the external inductance are underspecified values, and they are controllable in order that the LLC impedance has the inductive characteristics. The high coupling coefficient of 0.98 for the transformer was achieved by using the magnetic core and the effect of leakage inductances were relatively small.

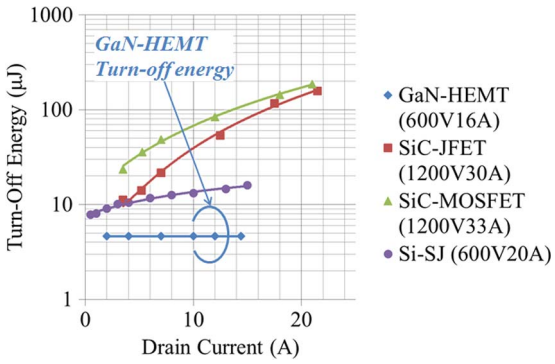

Fig. 7. Measurement results of turn-off switching loss energy for GaN-HEMT, Si-SJ MOSFET, SiC-JFET, and SiC-MOSFET.

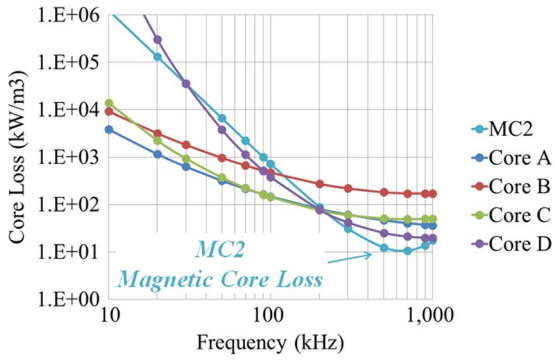

Fig. 8. Core losses generated from magnetic core materials. $\Delta B(\mathrm{mT}) \times f_{\mathrm{SW}}\,(\mathrm{kHz}) = 15\,000$.

B. Components for 1-MHz Operation

1) High-Speed and Ultra-Low-Loss Semiconductor Power Devices: The gallium nitride (GaN) power device is attractive to accomplish high efficiency and high-frequency operation. The switching loss energy is smaller than conventional Si power devices and the turn-off energy is independent of the drain current [20], [21]. In the LLC resonant converter topology, the turn-on energy can be eliminated by ZVS and the turn-off energy has to be minimized taking the turn-off time into account. The constant turn-off energy for the drain current makes the LLC converter design simple.

Fig. 7 shows the measurement result of the switching loss energy for GaN-HEMT, Silicon Carbide (SiC)-MOSFET, SiC-JFET and Si-SJ (Super Junction) MOSFET. The double-pulse test was applied to measure switching loss energies under the inductive load condition. The input drain to source voltage was dc 384 V and the drain current was varied to measure the losses. The 600 V SiC-SBD was utilized for the free-wheeling diode in this test.

The turn-off switching loss energies for SiC-MOSFET, SiC-JFET, and Si-SJ MOSFET increase as the drain current becomes larger. Characteristics, which the turn-off energy is independent of the drain current, can be seen in the turn-off switching loss energy of GaN-HEMT. The turn-off switching loss P_{OFF} generated from single GaN-HEMT in the connector is simply calculated as $P_{\mathrm{OFF}} = f_{\mathrm{SW}} \times E_{\mathrm{OFF}}$ by using the constant value E_{OFF} which means the turn-off switching loss energy in Fig. 7.

2) Low-Loss Magnetic Core Material for High-Frequency Transformer: Remarkable loss reduction of semiconductor power devices has been achieved by novel power devices such as SiC and GaN. The ratio of the power loss generated from magnetic components such as transformers and inductors becomes relatively increasing. To realize highly efficient contactless dc connector, the low-loss magnetic core material is indispensable for the high-frequency transformer. The core material MC2 from JFE Ferrite was utilized in this study.

Fig. 8 shows the core losses calculated for commercially available five magnetic core materials. The loss characteristics were obtained from published datasheets and the loss curves were drawn under the condition that the product of the magnetic flux density ΔB and switching frequency f_{SW} was 15 000. In Fig. 8, the core loss generated from the MC2 core material was minimum in case that the switching frequency was varied from 200 to 1000 kHz. This core material is one of the options to realize the high power density connector in the case of up to 1-MHz switching operation.

Here, the circuit parameter design and the material characteristics were described for 1.2-kW 384- to 192-V 1-MHz ICCC. In the next section, the power density and the conversion efficiency are estimated, and the potential for achieving higher power density is discussed.

IV. Design Consideration for High Power Density Contactless DC Connector

The design methodology for high power density converters has been already proposed [22]–[24]. The relationship between the power density and the efficiency is essential to evaluate the barrier of power converter performance. Authors have already proposed the design methodology for realizing high power density converters [24]. The parameter design to maximize the power density has been also conducted for the isolated dc–dc converter drawing relationship between the power density and the conversion efficiency using a power loss limit model for the novel power device and the loss map for the magnetic core material that estimate exact power losses under real circuit operation conditions [25]–[27]. Here, this design methodology is applied for the 1.2-kW 384- to 192-V contactless dc connector and the possible power density is estimated taking the influences of variable parameters related to the transformer into account.

A. Power Density and Conversion Efficiency Estimation

The relationship between the power density and the conversion efficiency of a 1.2-kW 384- to 192-V contactless dc connector is simply estimated under the ideal condition. The ideal condition means the following postulations.

- Semiconductor power devices, gate drivers and auxiliary circuits can be constructed by the highly integrated power modules.
- Power density is calculated by the total amount of components' pure volumes. The interspaces among components are not taken into account to estimate the power density.

Highly integrated power modules are now available, and the progress of the integration technology makes the effect of the interspace negligible. Through the aforementioned postulations, the influence of the design parameters related to the transformer on the connector performance can be simply discussed, and the potential of the connector using a GaN power transistor and an MC2 magnetic core material is shown clearly.

The power density of the connector D_P and the efficiency η are estimated simply by using the following equations:

$$D_P\left[\frac{W}{\mathrm{cm}^3}\right] = \frac{P_{\mathrm{OUT}}[W]}{V_{O_T}[\mathrm{cm}^3]} = \frac{P_{OUT}}{V_{O_M} + V_{O_X} + V_{O_C} + V_{O_{\mathrm{HS}}}(P_T)} \tag{7}$$

$$\eta[\%] = \frac{P_{\mathrm{OUT}}}{P_{\mathrm{OUT}} + P_T} \times 100. \tag{8}$$

The output power of the connector is P_{OUT} and the total volume of the connector is V_{OT}. The total volume V_{OT} consists of the volume of the power module V_{OM} including semiconductor power devices and the auxiliary circuit, the transformer volume V_{OX}, the resonant capacitor volume V_{OC} and the heat sink volume V_{OHS}. The heat sink volume V_{OHS} is simply estimated as follows by using the total power loss P_T and the heat dissipation efficiency k_{HS}[28]

$$V_{O_{\mathrm{HS}}}[\mathrm{cm}^3] = \frac{P_T[W]}{k_{\mathrm{HS}}[W/\mathrm{cm}^3]} = \frac{P_Q + P_X + P_C + P_D}{k_{\mathrm{HS}}} \tag{9}$$

$$P_Q[W] = P_{\mathrm{COND}} + P_{\mathrm{OFF}} = (R_{\mathrm{ON}} \cdot I^2 + f_{\mathrm{SW}} \cdot E_{\mathrm{OFF}}) \tag{10}$$

$$P_X[W] = P_{\mathrm{Cu}} + P_{\mathrm{CORE}} = \left\{(R_{\mathrm{WP}} + R_{\mathrm{WS}}) \cdot I^2 + f_{\mathrm{SW}} \cdot E_{\mathrm{CORE}})\right\} \tag{11}$$

$$P_C[W] = R_C \cdot I^2 \tag{12}$$

$$P_D[W] = V_D \cdot I. \tag{13}$$

The total power loss P_T consists of the loss from the main switch P_Q, the transformer loss P_X, the capacitor loss P_C and the loss from the rectifier diode P_D. The power losses from transistor P_Q consist of the conduction loss P_{COND} and the turn-off switching loss P_{OFF}. The conduction loss of the transistor P_{COND} depends on the on-resistance R_{ON} and the converter resonant current I. The turn-off switching loss P_{OFF} is determined by the operating switching frequency f_{SW} and the turn-off energy E_{OFF} shown in Fig. 7. The losses from the transformer P_X consists of the winding copper loss P_{Cu} and the core loss P_{CORE}. The copper loss P_{Cu} depends on the winding resistances R_{WP}, R_{WS} and the resonant current I. The core loss P_{CORE} is calculated by using the frequency f_{SW} and the core loss energy E_{CORE} in Fig. 8. The resistance R_{C} means the equivalent series resistance (ESR) of the resonant capacitor C and the voltage V_D shows the forward voltage drop of the rectifier diode D. Here, the current I through the resonant circuit is commonly utilized to estimate the losses P_Q, P_X, P_C and P_D because the turn ratio of the transformer n is 1.

TABLE III
PARAMETERS FOR HARDWARE IN CONTACTLESS DC CONNECTOR

Symbol	Meaning	Specification
Q_1, Q_2	GaN–HEMT	600 V, 16 A (Transphorm) R_{ON} = 150 mΩ
D_1–D_4	SiC–SBD	600 V, 12 A (Infineon) V_{D} = 1.4 V
X	Transformer Core	MC2 (JFE Ferrite)
	Transformer Winding	Polyurethane Enameled Copper Round Wire (UEW) ρ = 1.68 μΩ · cm J_{W} = 3 A/mm^2
C_{in}, C_{out}	MLCC	630 V, 22 μF (Murata)
C	MLCC	1000V, 3.3nF * 4(Murata)

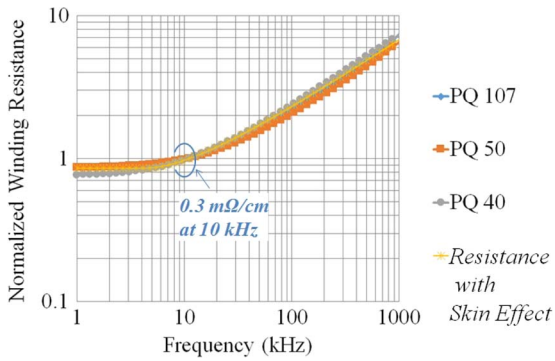

Fig. 9. Measurement result of normalized winding resistance per 1 cm in high-frequency transformer using PQ core.

B. Relationship Between Power Density and Efficiency for 1.2-kW 384- to 192-V Connector

The calculation result of the relationship between the power density and the efficiency are shown here for the 1.2-kW 384- to 192-V connector. Table III shows the hardware and their fixed parameters to develop the connector. Here, the 600 V-16 A GaN-HEMTs with on-resistance of 150 mΩ and 600 V-12 A SiC-SBDs with a forward voltage drop of 1.4 V at the rated current were utilized here. Their current densities were constant because the output power of 1200 W was constant in this design. The volume related to the power devices with auxiliary circuits are set at 15 cm^3 for the primary and the secondary circuits in the connector. The volume of 15 cm^3 was decided by using the datasheet of the commercially available 600 V-15 A power module and the integrated circuit board developed in the experiment.

The polyurethane enameled copper round wires (UEW) were applied for the transformer windings to decrease the winding resistance caused by the skin effect and the proximity effect [29]. The current density J_W of the primary and the secondary windings was also fixed at 3.0 A/mm^2 because of the constant output power. Fig. 9 shows the measurement result of the normalized winding resistances per 1 cm using the LCR meter PSM1735 from N4L in case the magnetic core shapes of PQ 40, PQ 50, and PQ 107 were employed for the high-frequency transformer X in the connector. Here, the resistance per 1 cm was 0.3 mΩ/cm at 10 kHz. The resistance with skin effect in this figure means the calculation result of the winding resistance, which takes the influence of the skin effect into account by using the analytical equation [30]. The calculation result

TABLE IV
PARAMETERS FOR DESIGN CONSIDERATION

Parameter	Min.	Max.	Step
Switching frequency	100 kHz	1 MHz	100 kHz
Magnetic Flux Density	50 mT	150 mT	10 mT
Transformer Core Shape	PQ20	PQ50	–
Core Width	20.0 mm	50.0mm	1.0 mm
Core Depth	14.0 mm	32.0 mm	–
Core Height	20.0 mm	50.0 mm	–
Heat Dissipation Efficiency		0.65 W/cm^3	

had good agreement with the measurement results for three cores. This means that the winding resistances per unit length could be exactly estimated by using the analytical equation taking the influences of the skin effect and the proximity effect into account. The winding resistances R_{WP} and R_{WS} of the transformer were calculated by using the calculation and the measurement results.

Table IV shows variable parameters for this design. The magnetic flux density ΔB, the core dimensions of the transformer and the switching frequency f_{SW} were varied. Parameters related to the transformer were mainly varied because the transformer had the some structural parameters, and these parameters affect the power loss and the volume directly. In this design, the heat dissipation efficiency k_{HS} was set at 0.65 W/cm^3. This was calculated by using the existing cooling condition of a 5-kW isolated dc–dc converter for 380-V dc distribution system [31]. The loss of the converter was 128 W from the efficiency of 97.5% and the heat sink volume was 200 cm^3.

To change the core shape, the core width was mainly controlled here. The core depth and the core height were considered to be proportion to the core width based on the determined core shape. The core shape of the transformer was fixed and the PQ type magnetic cores from PQ20 to PQ50 were applied for the connector design. The air gap between the primary and the secondary cores of the transformer is adjusted to prevent the saturation of the magnetic core, and this is much shorter than the dimensions of the magnetic core. The leakage inductances L_1 and L_2 might vary in case the core dimensions and the gap length changed. However, the utilization of the magnetic core makes their influences negligible because of the high coupling coefficient. In this paper, the leakage inductances L_1 and L_2 are relatively smaller than the required resonant inductance and the resonant inductance can be controlled independently from the outside. The influences of the resonant inductance on the connector performance is not considered because this inductance is sufficiently smaller than the magnetizing inductance of the transformer.

Fig. 10 shows the relationship between the power density and the efficiency for the 1.2-kW 384- to 192-V contactless dc connector in case that the switching frequency f_{SW} was varied from 100 to 1000 kHz, the magnetic flux density ΔB was varied from 50 to 150 mT, and the core dimensions were changed from PQ20 to PQ50. The power density and the efficiency were calculated for a total of 3000 samples (10 switching frequencies, 10 magnetic flux densities, and 30 transformer core shapes). In this figure, 1437 samples were plotted considering the maximum bias magnetic field to prevent the saturation of the transformer.

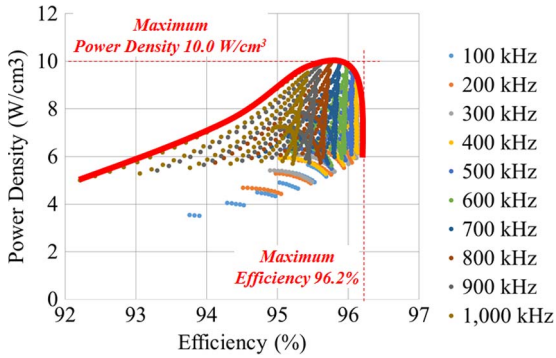

Fig. 10. Estimated power density and efficiency for 1.2-kW 384- to 192-V contactless dc connector.

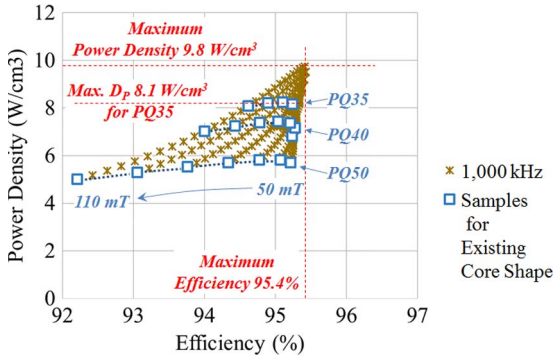

Fig. 11. Estimated power density and efficiency for contactless dc connector under 1000-kHz operation.

Parameters in Table IV affect both the power density and the efficiency largely. In the lower switching frequency operation (e.g., less than 500 kHz), the realization of the connector with the low power density and the high efficiency is expected. The maximum efficiency of 96.2% was confirmed at 400-kHz operation. In higher frequency operation (e.g., over 500 kHz), the connector with the higher power density and the lower efficiency will be feasible. The maximum power density of 10.0 W/cm^3 was shown at 800-kHz operation. In the switching frequency of 1.0-MHz operation, the power density of 9.8 W/cm^3 with the efficiency of 95.4% was the best solution.

Fig. 11 shows the power density and the efficiency under 1-MHz switching operation. These data were extracted from Fig. 10. The maximum power density of 9.8 W/cm^3 and the maximum efficiency of 95.4% were promising in this design. The data for the existing (commercially available) magnetic core of PQ35, PQ40, and PQ50 were also highlighted. The maximum power density was restricted by the variety of the product. In terms of the manufacturing, the utilization of the core shape PQ35 with the magnetic flux density ΔB of around 100 mT was the suitable operating condition to maximize the power density under 1.0-MHz operation. The power density of 8.1 W/cm^3 is expected in the experiment.

The power density and the efficiency were estimated and their relationship was clarified. The calculated power density of 8.1 W/cm^3 was maximum taking the experimental conditions into account although the power density of 10.0 W/cm^3 was promising in the whole design region of Table IV. In the next section, the prototype of the contactless dc connector based on the design consequence is developed to confirm the validity.

TABLE V
SPECIFICATIONS FOR EXPERIMENT

Symbol	Meaning	Value
P_{out}	Output power	1,200 W
V_{in}, V_{out}	Input / output voltage	384 V / 192 V
f_{sw}	Switching frequency	1 MHz
Q_1, Q_2	Main Switch	GaN–HEMT (Transphorm) 600 V, 16 A
D_1–D_4	Rectifier Diode	SiC–SBD (Infineon) 600 V, 12 A
X	Transformer	MC2 (JFE Ferrite) PQ35 Magnetic Core
N_P, N_S	Winding Turn Number for Transformer	$N_P = N_S = 5$
C	Resonant capacitor	MLCC (Murata) 1000 V, 3.3nF × 4

V. EXPERIMENTAL VERIFICATION OF CONTACTLESS DC CONNECTOR USING GAN-HEMT

The feasibility of the ICCC is verified experimentally here. The estimation result obtained from the design in the previous section was referred to decide the operation condition for the experiment. Table V shows the specifications for the experiment. This table was summarized by using Tables I to IV. The output power of the LLC resonant converter for the connector is 1.2 kW. The input and the output voltages are 384 and 192 V, respectively. The switching frequency was set at 1000 kHz because of the maximum frequency in the previous design. The switching operation at 1.0 MHz is sufficient to prove the feasibility under the several hundred of kilohertz operations. The estimated maximum power density of 9.8 $\mathrm{W/cm^3}$ under 1-MHz operation is approximately equal to the maximum power density of 10.0 $\mathrm{W/cm^3}$ in the whole design region.

The GaN-HEMTs and SiC-SBDs were utilized for semiconductor power devices and MC2 was employed for the magnetic core material of the high-frequency transformer to achieve high efficiency. The core shape was PQ35 and the turn number of the windings was set at 5 to keep the magnetic flux density ΔB of the transformer around 100 mT. The operating magnetic flux density ΔB can be calculated as the following equation. Here, the turn number of the transformer winding is N_P. The effective cross-sectional area of the magnetic core is S_e which is given from the datasheet. The injected voltage to the transformer is V_1 in Fig. 4. The induced time T_{ON} is determined by the switching frequency

$$\Delta \mathrm{B[T]} = \frac{1}{N_P \cdot S_e} \int_{T_{ON}} V_1 dt = \frac{1}{5 \cdot 196\ \mathrm{mm}^2} \cdot \frac{384}{2} \cdot \frac{1}{2 \cdot 1M} \cong 0.098\mathrm{T}. \quad (14)$$

Fig. 12 shows the fabricated prototype and Fig. 13 shows the steady-state waveforms under 1.2-kW and 1-MHz operation. The LLC input voltage means the drain to source voltage of the low-side GaN-HEMT. The LLC input current means the current through the leakage inductance L_1 and the resonant capacitor C. Rectifier input current is through the leakage inductance L_2. The constant output voltage of 192 V was obtained and the LLC input voltage was pure square wave, which changed from 0 to 384 V. The ZVS operation was confirmed because the LLC input voltage changed from 384 to 0 V when the LLC input current was positive. The ZCS was also confirmed because the rectifier input current was approximately equal to 0 A when the LLC input voltage changed.

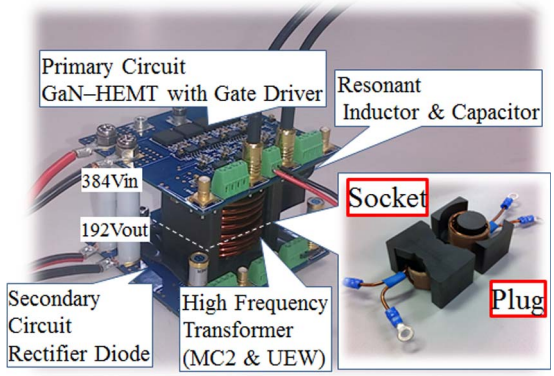

Fig. 12. Experimental breadboard for 1.2-kW 384- to 192-V contactless dc connector.

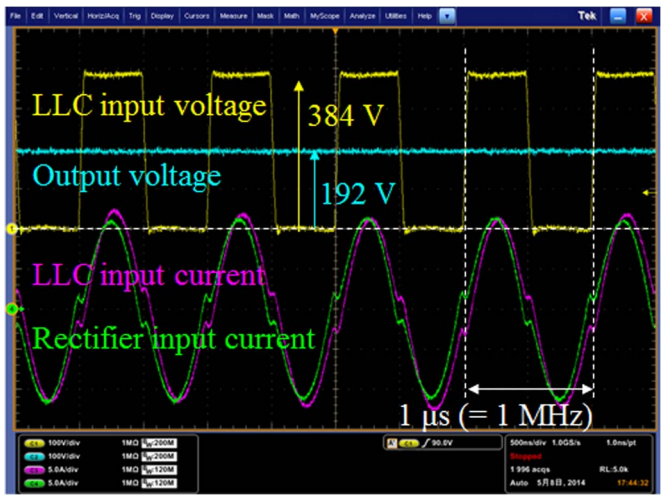

Fig. 13. Steady-state waveforms under 1200-W and 1000-kHz operation.

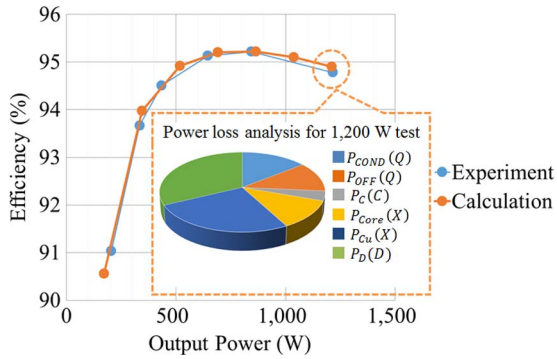

Fig. 14. Measurement and estimation results of conversion efficiency for 1.2-kW 384- to 192-V connector.

The measurement result of the conversion efficiency is shown in Fig. 14. The efficiencies from 200 to 1200 W were measured by using the power meter WT3000 from YOKOGAWA. From this figure, the maximum efficiency of 95.2% was confirmed at 850-W operation, and the efficiency of 94.9% was also shown at the rated power of 1200 W.

The calculation result of the power loss was also shown in Fig. 14. The conduction loss P_{COND} and the switching turn-off loss P_{OFF} generated from the transistor Q, the winding losses P_{Cu} and the core loss P_{CORE} from transformer X, the ESR loss P_{C} from the resonant capacitor C and the conduction loss P_{D} from the rectifier diode D were calculated based on the equations (10)—(13). The pie chart in this figure means the power loss analysis for the efficiency of 94.9% at 1200-W output power. These calculated results had good agreement with the experimental results from 200 W to 1.2 kW.

The ideal power density can be evaluated by using the experimental result at the rated power. The power loss P_{T} generated from the connector was 64.5 W because of the efficiency of 94.9% at 1.2 kW. The heat sink volume was calculated to be $99.2\ \mathrm{cm}^3$ from the heat dissipation efficiency of $0.65\ \mathrm{W/cm}^3$. The transformer volume V_{OX} was $34.3\ \mathrm{cm}^3$ from the published datasheet for PQ35. The volumes V_{OM} related to the semiconductor power devices with auxiliary circuits was $15.0\ \mathrm{cm}^3$ taking the circuit board in Fig. 12 and the commercially available 600 V-15 A integrated power module into consideration. From these data, the power density of $8.1\ \mathrm{W/cm}^3$ was obtained for the experimental breadboard. These were calculated by following equations:

$$P_T[W] = \left(\frac{100}{\eta[\%]} - 1\right) \cdot P_{\mathrm{OUT}}[W] = \left(\frac{100}{94.9} - 1\right) \cdot 1200 \cong 64.5\ \mathrm{W} \tag{15}$$

$$V_{O_{\mathrm{HS}}}[\mathrm{cm}^3] = \frac{P_T[W]}{k_{\mathrm{HS}}[W/\mathrm{cm}^3]} = \frac{64.5}{0.65} \cong 99.2\ \mathrm{cm}^3 \tag{16}$$

$$D_P\left[\frac{W}{\mathrm{cm}^3}\right] = \frac{P_{\mathrm{OUT}}[W]}{V_{O_T}[\mathrm{cm}^3]} = \frac{P_{\mathrm{OUT}}}{V_{O_M} + V_{O_X} + V_{O_C} + V_{O_{\mathrm{HS}}}} = \frac{1200}{15.0+34.3+0.05+99.2} \cong 8.1\ \mathrm{W/cm}^3. \tag{17}$$

The measured efficiency in the experiment had good agreement with the estimated one in the design. The power density obtained from the experiment also corresponded to the designed one. This means that the estimated power density and the efficiency in Fig. 10 will be achieved if the boundary conditions caused by the magnetic core dimensions in the real product are removed. The power density of $10.0\ \mathrm{W/cm}^3$ will be achieved under 800-kHz operation taking the aforementioned postulations for the design into account.

Design parameters that were fixed in this study has the potential to improve the power density of the ICCC. From Fig. 14, the conduction loss from the rectifier diode and the winding loss from the transformer were influential because these losses have large impact on the heat sink volume in the forced-air cooling. The utilization of Si-SBD is one of options to reduce the conduction loss from the rectifier diode [32]. The synchronous rectification is also the strong candidate for higher efficiency. For the winding loss reduction from the transformer, the copper foil winding will be attractive. The design consideration clarifies critical parameters to improve the power density, and the approach to achieve higher power density of over $10.0\ \mathrm{W/cm}^3$ can be discussed by taking these parameters into account.

VI. Conclusion

The ICCC has been proposed to realize the future high power density 380-V dc distribution system in data centers. The LLC resonant circuit topology was applied to realize the short-range highly efficient contactless power transfer. The prototype of a 1200-W 384- to 192-V ICCC was fabricated using the GaN-HEMT and MC2. The efficiency of over 95.0% was experimentally confirmed and the power density of $8.1\ \mathrm{W/cm}^3$ was obtained. The design consideration for the contactless dc connector was also conducted, and the approach to achieve higher power density of $10.0\ \mathrm{W/cm}^3$ was shown. This means that the proposed ICCC will be developed in the same volume with the conventional metal contact connector, and the conventional connector will be removed for space saving.

The contactless dc connector has the potential to realize the function of the protection device as the current limiter because this is derived from the isolated dc–dc converter. The proposed connector contributes to realizing highly efficient, space saving, and reliable future dc distribution system.

References

[1] R. R. Schmidt *et al.*, "Evolution of data center environmental guidelines," *ASHRAE Trans.*, vol. 110, pt. 1, pp. 559–566, 2004.

[2] T. Babasaki *et al.*, "Developing of higher voltage direct-current power-feeding prototype system," in *Proc. INTELEC*, Incheon, Korea, 2009, pp. 1–5.

[3] A. Matsumoto, A. Fukui, T. Takeda, and M. Yamasaki, "Development of 400-Vdc output rectifier for 400-Vdc power distribution system in telecom sites and data centers," in *Proc. INTELEC*, Incheon, Korea, 2010, pp. 1–6.

[4] Y. Sugiyama, "Green ICT toward low carbon society-green R&D activities in NTT," in *Proc. 4th Int. Workshop Green Commun.*, Kyoto, Japan, 2011, pp. 1–49.

[5] T. Ninomiya, Y. Ishizuka, R. Shibahara, and S. Abe, "Energy-saving technology using next-generation power electronics," (in Japanese), in *Proc. IEE-Japan Ind. Appl. Soc. Conf.*, Chiba, Japan, 2012, pp. I15–I20.

[6] B. Eckardt, A. Hofmann, S. Zeltner, and M. Maerz, "Automotive power-train DC/DC converter with 25 $\mathrm{kW/dm}^3$ by using SiC diodes," in *Proc. 4th Int. CIPS*, Naples, Italy, 2006, pp. 1–6.

[7] J. Sun, M. Xu, Y. Ying, and F. C. Lee, "High power density, high efficiency system two-stage power architecture for laptop computers," in *Proc. 37th IEEE PESC*, Jeju, Korea, 2006, pp. 231–237.

[8] J. Biela, U. Badstuebner, and J. W. Kolar, "Design of a 5 kW, 1U, 10 kW/ltr. resonant DC-DC converter for telecom applications," in *Proc. INETELEC*, Rome, Italy, 2007, pp. 824–831.

[9] Y. Hayashi, H. Toyoda, T. Ise, and A. Matsumoto, "Contactless DC connector based on ISOP-IPOS topology for high power density 380 V DC power feeding system," in *Proc. 16th EPE-ECCE Europe*, Lappeenranta, Finland, 2014, pp. 1–10.

[10] J. W. Kolar and G. Ortiz, "Solid-state-transformers: Key components of future traction and smart grid systems," in *Proc. IPEC ECCE Asia*, Hiroshima, Japan, 2014, pp. 22–35.

[11] M. Kasper, D. Bortis, J. W. Kolar, and G. Deboy, "Hyper-efficient (98%) and super-compact (3.3 kW/dm3) isolated AC/DC telecom power supply module based on multi-cell converter," in *Proc. IEEE ECCE*, Pittsburgh, PA, USA, 2014, pp. 150–157.

[12] D. A. G. Pedder, A. D. Brown, and J. A. Skinner, "A contactless electrical energy transmission system," *IEEE Trans. Ind. Electron.*, vol. 46, no. 1, pp. 23–30, Feb. 1999.

[13] E. Kim, S. Kang, K. Yoon, and Y. Kim, "A contactless power supply for photovoltaic power generation system," in *Proc. IEEE APEC*, Austin, TX, USA, 2008, pp. 1910–1913.

[14] Y. Hayashi, "High power density rectifier for highly efficient future DC distribution system," *J. Elect. Eng. Res. (EER)*, vol. 1, no. 3, pp. 49–59, Jul. 2013.
[15] [Online]. Available: http://www.vicorpower.com
[16] Y. Hayashi, "Multi-converter approach to higher power density DC-DC converter for 380 V DC distribution system," *J. Energy Power Eng. (JEPE)*, vol. 7, no. 7, pp. 1371–1343, Jul. 2013.
[17] T. S. Chan and C. Chern-Lin, "LLC resonant converter for wireless energy transmission system with PLL control," in *Proc. IEEE ICSET*, Singapore, 2008, pp. 136–139.
[18] Y. Yang, "A contactless charger with LLC tank and microcontroller," in *Proc. 35th IEEE IECON*, Porto, Portugal, 2009, pp. 3761–3766.
[19] H. S. Choi, "Design consideration of half-bridge LLC resonant converter," *J. Power Electron.*, vol. 7, no. 1, pp. 13–20, Jan. 2007.
[20] Z. Liu, X. Huang, F. C. Lee, and Q. Li, "Simulation model development and verification for high voltage GaN HEMT in cascode structure," in *Proc. IEEE ECCE*, Denver, CO, USA, 2013, pp. 3579–3586.
[21] W. Zhang *et al.*, "Evaluation of 600 V Cascode GaN HEMT in device characterization and All-GaN-based LLC resonant converter," in *Proc. IEEE ECCE*, Denver, CO, USA, 2013, pp. 3571–3578.
[22] J. W. Kolar, J. Biela, and J. Miniböck, "Exploring the pareto front of multi-objective single-phase PFC rectifier design optimization −99.2% Efficiency versus 7 kW/din3 power density," in *Proc. IEEE 6th IPEMC*, Wuhan, China, 2009, pp. 1–21.
[23] H. Ohashi, "Research activities of the power electronics research center with special focus on wide band gap materials," in *Proc. 4th CIPS*, Naples, Italy, 2006, pp. 1–4.
[24] Y. Hayashi, K. Takao, and H. Ohashi, "Fundamental study of high density DC/DC converter design based on sensitivity analysis," in *Proc. INTELEC*, Incheon, Korea, 2009, pp. 1–5.
[25] K. Takao, H. Irokawa, Y. Hayashi, and H. Ohashi, "Novel exact power loss design method for high output power density converter," in *Proc. 37th IEEE PESC*, Jeju, Korea, 2006, pp. 2651–2655.
[26] S. Iyasu, T. Shimizu, and K. Ishii, "A novel inductor loss calculation method on power converters based on dynamic minor loop," *IEEJ Trans. Ind. Appl.*, vol. 126-D, no. 7, pp. 1028–1034, 2006.
[27] K. Kim and T. Shimizu, "Dynamic iron loss measurement method for an AC filter inductor on a PWM inverter," in *Proc. 12th Eur. Conf. EPE*, Aalborg, Denmark, 2007, pp. 1–9.
[28] M. Tsukuda, I. Omura, T. Domon, W. Saito, and T. Ogura, "Demonstration of high output power density (30 W/cc) converter using 600 V SiC-SBD and low impedance gate driver," in *Proc. IPEC*, Niigata, Japan, 2005, pp. S32–S34.
[29] S. Ojika, Y. Miura, and T. Ise, "Inductive contactless power transfer system with coaxial coreless transformer for DC power distribution," in *Proc. 5th Annu. Int. Energy Convers. Congr. Expo. Asia/Pac. Reg.*, Melbourne, Australia, 2013, pp. 1046–1051.
[30] N. Idir, Y. Weens, and J. Franchaud, "Skin effect and dielectric loss models of power cables," *IEEE Trans. Dielect. Elect. Insul.*, vol. 16, no. 1, pp. 147–154, Feb. 2009.
[31] Y. Hayashi and M. Mino, "An approach to a higher-power-density power supply for a 380-V DC distribution system," *Elect. Eng. Japan*, vol. 186, no. 3, pp. 51–62, Feb. 2014.
[32] Y. Hayashi, H. Toyoda, T. Ise, and A. Matsumoto, "Design consideration for contactless DC connector in high power density future 380 V DC distribution system," in *Proc. IEEE Energy Convers. Congr. Expo.*, Pittsburgh, PA, USA, 2014, pp. 5690–5697.

Yusuke Hayashi was born in 1977. He received the B.Eng., M.Eng. and Doctor of Engineering degrees in electrical engineering from Osaka University, Osaka, Japan, in 1999, 2001 and 2004 respectively.

He joined the National Institute of Advanced Industrial Science and Technology (AIST), Power Electronics Research Center, Tokyo, Japan, in April 2004, and he joined NTT Facilities in April 2009. Since May 2013, he has been with Osaka University. He is engaged in research and development of power converter control in distribution systems and the design methodology for high power density converter using SiC and GaN power devices. Currently, he is mainly engaged in the development of high power density dc power supplies for 380-V dc distribution systems.

Hajime Toyoda was born in 1991. He received the B.Eng. degree in electrical engineering from Ritsumeikan University, Siga, Japan, in 2013. In April 2013, he entered the master's program of the Division of Electrical, Electronic and Information Engineering, Osaka University, Osaka, Japan.

His research concerns dc power connectors using LLC resonant circuits.

Toshifumi Ise was born in 1957. He received the B.Eng., M. Eng., and Doctor of Engineering degrees in electrical engineering from Osaka University, Osaka, Japan, in 1980, 1982, and 1986, respectively.

Since 1990, he has been with the Faculty of Engineering, Osaka University. Currently, he is a Professor with the Division of Electrical, Electronic and Information Engineering, Graduate School of Engineering, Osaka University. From 1986 to 1990, he was with Nara National College of Technology, Nara, Japan. His research interests are in the areas of power electronics and applied superconductivity for power systems including superconducting magnetic energy storage, and future power systems, including distributed generation.

Akira Matsumoto was born in 1977. He received the B.Eng. and the M. Eng. degrees in electrical engineering from Tohoku University, Sendai, Japan, in 2001 and 2003, respectively.

He joined NTT Facilities, Tokyo, Japan, in 2003, and is currently with the Research and Development Headquarters. His research interests are in the areas of electric power systems, dc distribution systems, and power quality.